NEON NORMALISZED DIFFERENCE VEGETATION INDEX (NDVI), ENHANCED VEGETATION INDEX (EVI), ATOMOSPHERICALLY RESISTANT VEGETATION INDEX (ARVI), CANOPY XANTHOPHYLL CYCLE (PRI), AND CANOPY LIGNIN (NDLI) ALGORITHM THEORETICAL BASIS DOCUMENT

PREPARED BY	ORGANIZATION	DATE
David Hulslander	AOP	5/13/2015

APPROVALS	ORGANIZATION	APPROVAL DATE
Kate Thibault	SCI	03/25/2022

RELEASED BY	ORGANIZATION	RELEASE DATE
Tanisha Waters	CM	03/25/2022

See configuration management system for approval history.

The National Ecological Observatory Network is a project solely funded by the National Science Foundation and managed under cooperative agreement by Battelle. Any opinions, findings, and conclusions or recommendations expressed in this material are those of the author(s) and do not necessarily reflect the views of the National Science Foundation.

Change Record

REVISION	DATE	ECO #	DESCRIPTION OF CHANGE
A	01/28/2016	ECO-03481	Initial release
B	03/25/2022	ECO-06791	• Revised logo • Minor formatting updates

TABLE OF CONTENTS

LIST OF TABLES AND FIGURES

1 DESCRIPTION

1.1 Purpose

This document details the algorithms and processes used for creating NEON Level 2 data products NDVI, EVI, Canopy Xanthophyll Cycle, and Canopy Lignin from Level 1 reflectance data. Data Product Identifiers are provided in **Table 1**. Where necessary, this document includes a detailed discussion of appropriate theoretical background, data product provenance, quality assurance and control methods used, approximations and/or assumptions made, and an exposition of uncertainty resulting in a cumulative reported uncertainty for this product.

1.2 Scope

This document describes the theoretical background and entire algorithmic process for creating NEON Level 2 data products NDVI, EVI, Canopy Xanthophyll Cycle, and Canopy Lignin from Level 1 reflectance data (RD[03]). It does not provide computational implementation details, except for cases where these stem directly from algorithmic choices explained here.

2 RELATED DOCUMENTS AND ACRONYMS

2.1 Applicable Documents

AD [01]	NEON.DOC.000001	NEON Observatory Design
AD [02]	NEON.DOC.002652	NEON Level 1, Level 2 and Level 3 Data Products Catalog
AD [03]	NEON.DOC.005005	NEON Level 0 Data Product Catalog
AD [04]	NEON.DOC.002236	AOP Overview Document
AD [05]	NEON.DOC.015015	AOP Payload Integration Mount Design

2.2 Reference Documents

RD [01]	NEON.DOC.000008	NEON Acronym List
RD [02]	NEON.DOC.000243	NEON Glossary of Terms
RD [03]	NEON.DOC.001288	NEON Imaging spectrometer radiance to reflectance algorithm theoretical basis document
RD [04]	NEON.DOC.001290	NEON Algorithm Theoretical Basis Document: Imaging Spectrometer Geolocation Processing
RD [05]	NEON.DOC.001210	NEON Algorithm Theoretical Basis Document: NEON Imaging Spectrometer Level 1B Calibrated Radiance

2.3 Verb Convention

"Shall" is used whenever a specification expresses a provision that is binding. The verbs "should" and "may" express non-mandatory provisions. "Will" is used to express a declaration of purpose on the part of the design activity.

3 DATA PRODUCT DESCRIPTION

3.1 Variables Reported

The primary outputs from the NEON Imaging Spectrometer (NIS) NDVI, EVI, ARVI, Canopy Xanthophyll Cycle and Canopy Lignin algorithms include:

- NDVI Image File: This is the first band in the ENVI format Vegetation Indices file
- EVI Image File: This is the second band in the ENVI format Vegetation Indices fie
- ARVI Image File: This is the third band in the ENVI format Vegetation Indices file
- Canopy Xanthophyll Cycle Image File: This is the fourth band in the ENVI format Vegetation Indices file
- Canopy Lignin Image File: This is the fifth band in the ENVI format Vegetation Indices file

The ENVI file format consists of a flat binary file (*.dat) containing the 4-byte floating point pixel data values in band sequential (BSQ) interleave with an accompanying human-readable formatted ASCII text file (*.hdr), ("ENVI Image Files (Using ENVI) | Exelis VIS Docs Center," n.d.).

3.2 Input Dependencies

A NIS Level 1B reflectance dataset is the only required input for creating the NDVI, EVI, Canopy Xanthophyll Cycle and Canopy Lignin data products.

3.3 Product Instances

The NEON data products produced directly from these algorithms are:

Table 1. Data Products generated by Algorithms described in this ATBD.

Data Product Identification Code	Data Product Name
NEON.DOM.SITE.DP2.30026	Vegetation Indices – Spectrometer
NEON.DOM.SITE.DP2.30020	Canopy Xanthophyll Cycle
NEON.DOM.SITE.DP2.30022	Canopy Lignin

3.4 Temporal Resolution and Extent

The NIS vegetation index algorithms are applied on each AOP flight line, which typically measure between 5 and 20 km in length and approximately 600 m in width. Flight speeds are typically around 100 knots (185.2 km/hour), and therefore, the time required to acquire flight lines of the lengths stated will range from 1.6 to 6.5 minutes. The integration time for the NIS detector array is 100 milliseconds, so a time integrated observation is acquired every 100 milliseconds along-track.

3.5 Spatial Resolution and Extent

The NIS vegetation index algorithms are applied on each AOP flight line, which typically measure between 5 and 20 km in length and approximately 600 m in width, at 1000 m flying altitude. The

Instantaneous Field of View (IFOV) of the NEON Imaging Spectrometer is 1.0 milliradian, which equates to a ground sampling distance at a nominal flight of 1000 m above ground, of 1 meter at nadir. The actual ground resolution will vary with flight altitude and cross-track field angle.

4 SCIENTIFIC CONTEXT

NEON's Airborne Observation Platform (AOP) remote sensing payload includes the NEON Imaging Spectrometer (NIS), a visible-to-shortwave infrared (VSWIR) pushbroom sensor; a small-footprint full waveform LiDAR, and a high-resolution digital camera (AD [04]). The instrument payload is mounted onto a common integration plate, the Platform Integration Mount, or PIM (AD [05]). The entire AOP remote sensing payload is integrated onto a de Havilland DHC-6 Twin Otter aircraft configured with a large open downward-looking viewport. The payload is mounted directly on the cabin floor via the seat rails with the sensors viewing in the nadir direction through an open port. Imaging spectrometer data acquired with the NIS instrument supports the creation of derived data products which give unique insight in to the types, abundance, and quality of various land covers, including vegetation (Govender, Chetty, & Bulcock, 2007 and).

4.1 Theory of Measurement/Observation

Level 1 NIS reflectance data provide reflectance spectra for each pixel in 424 discrete 5 nm bandpasses for wavelengths from 382 nm to 2512 nm (RD[05]). The unique reflectance spectra of materials on the ground are captured in this data. As full spectral curves are difficult and cumbersome to process and analyze, applications typically utilize only those spectral regions relevant to the materials or phenomena of interest and their key spectral features. This approach also works well with the much broader bandpasses of multispectral sensors. For vegetation, these spectral features and regions include blue reflectance, the green vegetation reflectance feature and its shoulders, the chlorophyll absorption feature in the red wavelengths, the near infrared (NIR) shoulder, and the lignin reflectance feature in the shortwave infrared (SWIR). The regions are shown in **Figure 1** in the larger context of the electromagnetic spectrum as well as how they relate to the commonly used Landsat 7 and 8 bandpasses.

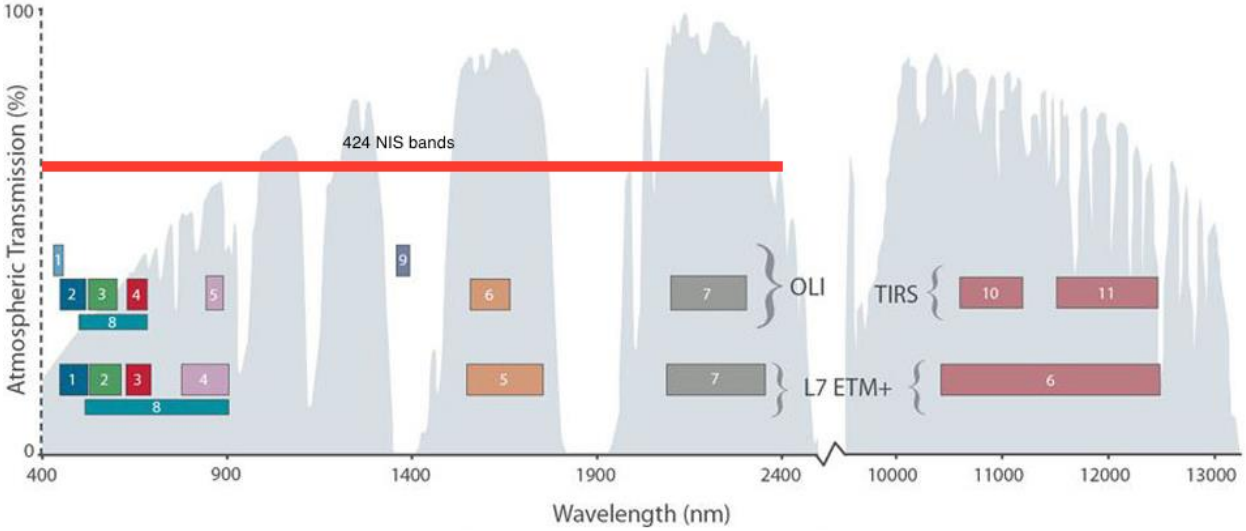

Figure 1. Portions of the electromagnetic spectrum showing% atmospheric transmission and the bandpasses for Landsat 7 (ETM+) and Landsat 8 (OLI and TIRS) sensors. Landsat 8 OLI Bands 2, 3, 4, and 5 correspond to Blue,

Green, Red and Near Infrared (NIR), respectively. Landsat has used 4 to 9 bands, depending on generation, to cover the roughly 400 to 2400 nm portion of the spectrum here, which is covered by the NEON Imaging Spectrometer with 424 5-nm-wide bands. (USGS, 2013)

For spectral indices, the reflectance values of those regions are combined using various functions, typically as normalized ratios of two or more bands. This reduces the data volume to a single value per pixel directly related to the topic of study and comparable across both space and time and even between different sensors and datasets. Using ratios can also help reduce error, as it is inherently a relative measure and eliminates error common to the absolute measure of the bands involved. Many such indices are now common in remote sensing and the earth sciences, including but not limited to (Miura et al, 2011):

- Normalized Difference Vegetation Index (NDVI)
- Enhanced Vegetation Index (EVI)
- Atmospherically Resistant Vegetation Index (ARVI)
- Canopy Xanthophyll, or Photochemical Reflectance Index (PRI)
- Canopy Lignin, or Normalized Difference Lignin Index (NDLI)

4.2 Theory of Algorithm

Though they differ in the phenomenology on which they focus, all vegetation indices have the same basic approach of using 2 to 4 spectral bands related to reflectance or absorption by specific compounds and combining those bands in normalized, unitless ratios. The following subsections, one per index covered in this document, detail the theory behind each index's particular ratio algorithm. Exact NIS bands used are also named in each section. Currently, NIS bands are selected to most closely match the center of historically used broader multispectral ranges or most closely match the specified band(s) for the index as specified in the index's original publication as noted.

4.2.1 Normalized Difference Vegetation Index (NDVI)

The Normalized Difference Vegetation Index (NDVI) is a measure of dense green vegetation. It has been a widely popular vegetation index for over 40 years (Mercanti, 1974). Values of NDVI range from -1 to 1, with green vegetation concentrating in the range of 0.2 to 0.8. Two advantages behind the theory of NDVI are that it combines a normalized difference formulation and uses the highest absorption and reflectance regions of chlorophyll. In practice, this has been found to make NDVI very robust over a wide range of conditions. In regions of dense vegetation and high LAI, however, it can produce saturated values. The ideal NDVI algorithm is given in equation Eq. 1. NIS1 bands at 648.2 nm (channel 54) and 858.6 nm (channel 96) are used for Red, and NIR respectively. These bands correspond to the center of the multispectral bandpasses used for NDVI historically (Mercanti, 1974).

$$NDVI = \frac{(NIR - Red)}{(NIR + Red)} \qquad \textbf{Eq. 1}$$

4.2.2 Enhanced Vegetation Index (EVI)

The Enhanced Vegetation Index (EVI) was developed as a standard MODIS product (Huete, Justice, & Van Leeuwen, 1999). Its design aims to improve the NDVI by optimizing the vegetation signal in higher LAI regions in which NDVI frequently saturates. The blue region of the spectrum is used in EVI to help compensate for soil background signals as well as to reduce atmospheric influences (e.g. aerosol scattering). EVI, like NDVI, is a normalized ratio and therefore also ranges in value from -1 to 1. The ideal EVI algorithm is given in Eq. 2. NIS1 bands at 467.8 nm (channel 18), 648.2 nm (channel 54), and 858.6 nm (channel 96) are used for Blue, Red, and NIR respectively.

$$EVI = 2.5 * \frac{(NIR - Red)}{(NIR + 6 * Red - 7.5 * Blue + 1)} \quad \textbf{Eq. 2}$$

4.2.3 Atmospherically Resistant Vegetation Index (ARVI)

The Atmospherically Resistant Vegetation Index (ARVI) is an enhancement to NDVI designed to make it relatively more resistant to atmospheric factors, including atmospheric aerosol levels (Kaufman & Tanre, 1992). It uses reflectance values from the blue region of the spectrum to correct red reflectance values for atmospheric scattering effects. ARVI is most useful in geographic regions of high atmospheric aerosol content, e.g. tropical regions experiencing high soot levels associated with agricultural burning operations. The ideal ARVI algorithm is given in Eq. 3. NIS1 bands at 467.8 nm (channel 18), 648.2 nm (channel 54), and 858.6 nm (channel 96) are used for Blue, Red, and NIR respectively.

$$ARVI = \frac{NIR - [Red - \gamma(Blue - Red)]}{NIR + [Red - \gamma(Blue - Red)]} \quad \textbf{Eq. 3}$$

The gamma constant is a weighting constant whose value is set depending on aerosol type and degree of atmospheric compensation. When atmospheric correction has been performed, a value of 1 for gamma is commonly used. NEON adjusts L1 data for atmospheric effects (including aerosols) using ATCOR prior to calculating ARVI (RD[03]).

As a normalized ratio index, the value of ARVI ranges from -1 to 1, with higher pixel values corresponding to healthier and greener vegetation.

4.2.4 Canopy Xanthophyll (PRI)

Canopy Xanthophyll, or Photochemical Reflectance Index (PRI), is a reflectance ratio index that is sensitive to changes in carotenoid pigments, particularly xanthophyll pigments, in live foliage (Gamon, Penuelas, & Field, 1992). Carotenoid pigments are proxies for photosynthetic light use efficiency, or the rate of carbon dioxide uptake by foliage per unit energy absorbed. As such, it is used in studies of vegetation productivity and stress. Applications include vegetation health in evergreen shrublands,

forests, and agricultural crops prior to senescence. PRI ranges from -1 to 1, with green vegetation pixels ranging from -0.2 to 0.2. The ideal Canopy Xanthophyll algorithm is given in Eq. 4. NIS1 bands at 532.9 nm (channel 31) and 568.0 nm (channel 38) are used for ρ_{531} and ρ_{570} respectively.

$$PRI = \frac{\rho_{531} - \rho_{570}}{\rho_{531} + \rho_{570}} \quad \text{Eq. 4}$$

4.2.5 Canopy Lignin (NDLI)

Canopy Lignin, or Normalized Difference Lignin Index (NDLI), estimates the relative amounts of lignin contained in vegetation canopies. Leaf lignin concentration and canopy foliage biomass are the determining factors for vegetation reflectance spectra at 1754 nm. NDLI uses leaf lignin concentration and canopy foliar biomass, as combined in the 1750 nm range, as a means for predicting total canopy lignin content. NDLI is most frequently use for ecosystem analysis and detection of surface plant litter. NDLI is a relatively new index in remote sensing and the earth sciences and considered somewhat experimental (Serrano, Penuelas, & Ustin, 2002).

The ideal NDLI algorithm is given in Eq. 5. NIS1 bands at 1680.1 nm (channel 260) and 1755.3 nm (channel 275) are used for ρ_{1680} and ρ_{1754} respectively.

$$NDLI = \frac{\log\left(\frac{1}{\rho_{1754}}\right) - \log\left(\frac{1}{\rho_{1680}}\right)}{\log\left(\frac{1}{\rho_{1754}}\right) + \log\left(\frac{1}{\rho_{1680}}\right)} \quad \text{Eq. 5}$$

4.3 Special Considerations

While the equations for these indices are well settled and agreed upon, the exact wavelength ranges or bandpasses to be used in each are largely undetermined. Most vegetation index products are constrained to the larger bandpasses of the multispectral instruments for which they are developed, e.g. Landsat and MODIS "blue", "red", and "NIR" bands. Historically, researchers using hyperspectral instruments such as AVIRIS have chosen either single bands closest to the band centers of the popular multispectral bandpasses mentioned above, or have used a weighted resampling of a number of the hyperspectral bands to mimic the broader multispectral bandpasses (Vane, 1988).

The NIS instrument, however, provides a new level of flexibility in choosing which spectral bands to choose in calculating band indices and ratios. Where a multispectral sensor may offer one band for "NIR", NIS will offer a selection from 1 to tens of bands that may be used, excluded, or combined in various ways.

For current implementation of vegetation index products, NEON will be using single NIS bands closest to the band centers of the relevant traditional multispectral bands. NEON will be optimizing the combination of NIS channels in production implementation of these indices. The combination of channels will be chosen to best capture the spectral features required for each index, e.g. the chlorophyll absorption in the red region, rather than mimicking other sensors. Indices calculated to match other sensor index products will be produced separately.

5 ALGORITHM IMPLEMENTATION

The processing of the NIS reflectance data to the vegetation indices data is achieved in the steps shown in the left column of **Figure 2**. The engineering grade NIS vegetation index algorithms have been implemented in IDL and use the ENVI API for data access and processing.

Inputs: NEON Imaging Spectrometer L1 Orthorectified Surface Directional Reflectance data product (NEON.DOM.SITE.DP1.30006).

The IDL code for performing the calculations of vegetation indices is in Appendix .

As each of the three NIS instruments is individually made, the matching of spectral bands to pixels will not be identical. To ensure compatibility of vegetation index products across the sensors, the bands used for calculating the indices are chosen to be those closest to the centers as defined in the literature. The desired band centers used for the indices are:

Table 2. Common names for bands used in vegetation indices and their optimal center wavelengths.

Band Name	Index/Indices using this band	Desired band center (nm)
Blue	EVI, ARVI	470
PRI 1	Canopy Xanthophyll (PRI)	531
PRI 2	Canopy Xanthophyll (PRI)	570
Red	NDVI, EVI, ARVI	650
NIR	NDVI, EVI, ARVI	860
Lignin 1	Canopy Lignin (NDLI)	1680
Lignin 2	Canopy Lignin (NDLI)	1754

After the band center is mapped to a specific pixel, additional pixels around the central wavelength pixel are co-added and weighted to meet the desired spectral bandpass for the given spectral band. Optimal bandwidths for the bandpasses vary from one vegetation index to the next. NIS 5 nm bandpasses allow for very precise targeting of the spectral features required for each index and in some cases, e.g. NDLI, are the standard in research and industry. Other indices, e.g. NDVI, EVI, and ARVI, were designed for the much broader bandpasses found in orbital multispectral sensors such as MODIS and Landsat. NEON will be investigating and implementing combining multiple NIS bands in to wider bandpasses for use in these indices. Early indications are that combining several NIS bands may provide a more robust and cross-sensor compatible product while helping to minimize uncertainty.

6 UNCERTAINTY

As the vegetation index products described in this document are all entirely derived from L1 NIS surface reflectance data combined in normalized ratios, their uncertainties are therefore entirely dependent on the uncertainty in the L1 reflectance data and the combinations and ratios of bands used in each index. Additional sources of errors or uncertainties will be included in analysis as they are identified during the course of observatory construction and operation. There are a number of sources of uncertainty contributing to the reflectance data product uncertainty, as shown in **Figure 2**. The detailed analysis of uncertainty in the reflectance data is discussed in the L1 Reflectance ATBD. The reported uncertainty values from the L1 Reflectance ATBD are used here. A summary of them is in **Table 3**.

Table 3. Summary of expected reflectance uncertainties due to site and observing conditions, data acquisition procedures, instrumentation nature, and data processing requirements.

Data Quality	Surface Type	Atmospheric Conditions	ρ Error (% reflectance)
Ideal	Well characterized, low complexity	Well characterized, spatially and temporally consistent, clear	± 2%
Medium	Moderately complex, moderately well characterized	Some spatial and temporal variation, moderate haze and aerosol	± 5%
Low	Highly complex and/or poorly characterized	Poorly characterized, highly variable, anomalous conditions	± 10%

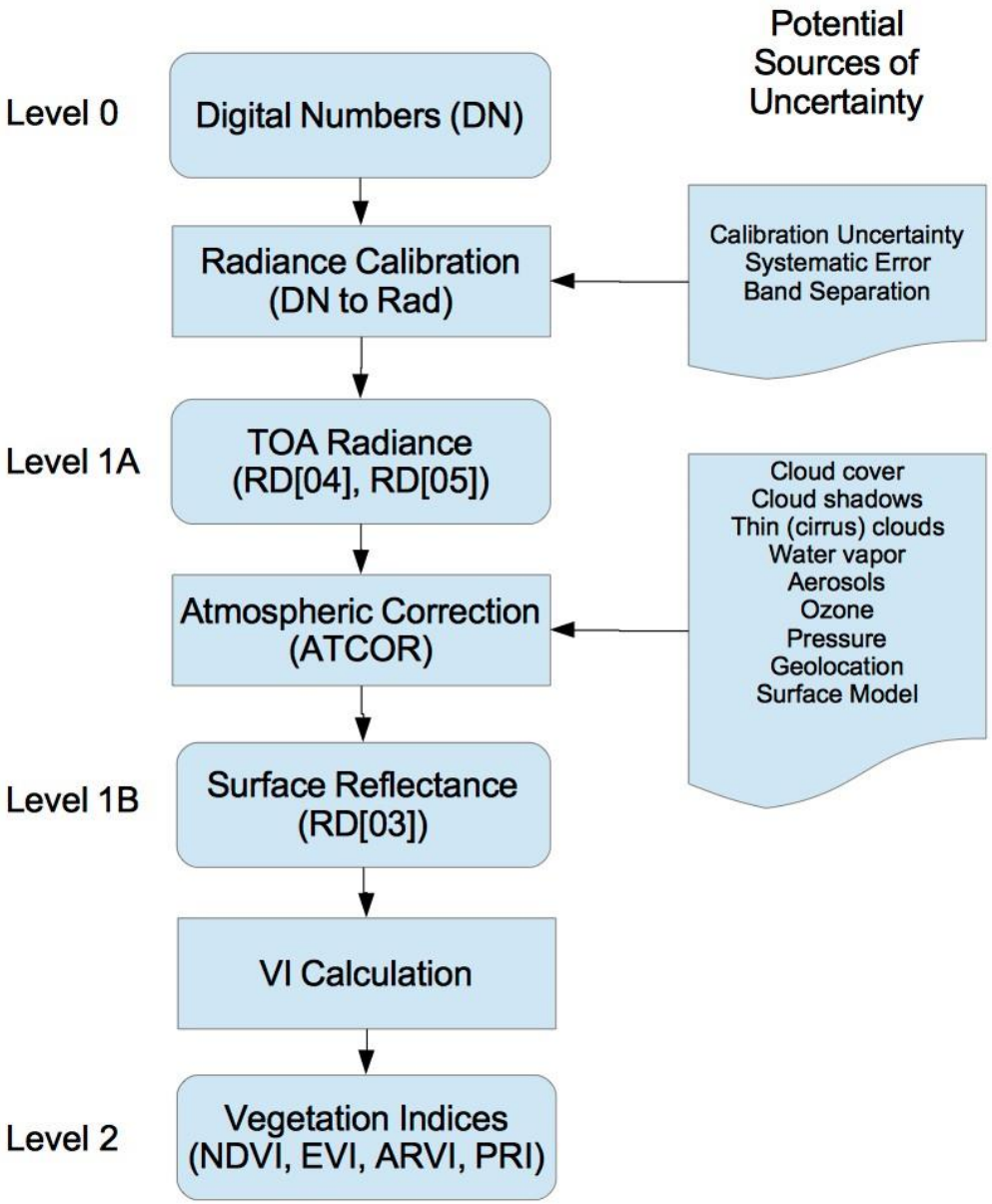

Figure 2. End-to-end analysis of vegetation index uncertainty including sources of uncertainty in upstream processing and systems contributing to the reflectance data input required for calculating vegetation indices.

6.1 Analysis of Uncertainty

Propagation and accumulation of uncertainty from sources in to the vegetation index products can be modeled using the "law of propagation of uncertainty" (NCSL, 1997, Taylor and Kuyatt, 1994). This approach handles only random errors, does not consider systematic biases, and assumes statistical independence in the errors. Systematic errors and biases are addressed in the processing of the raw NIS data to the surface reflectance values used here (RD[03], RD[04], RD[05]). As has been done with MODIS vegetation indices, we use the framework of vegetation indices being a quantity of interest y based on a function combining estimates of n other quantities as shown in Eq. 6 (Huete et al., 1999).

$$y = f(x_1, x_2, \ldots, x_n) \qquad \textbf{Eq. 6}$$

An uncertainty propagation equation, Eq. 7, can be based on a first-order Taylor series expansion of Eq. 6, where u is uncertainty (Huete et al., 1999).

$$u^2 = \sum_{i=1}^{n}\sum_{j=1}^{n} \frac{\partial f}{\partial x_i}\frac{\partial f}{\partial x_j} u(x_i, x_j) = \sum_{i=1}^{n} \left(\frac{\partial f}{\partial x_i}\right)^2 u^2(x_i) + 2\sum_{i=1}^{n-1}\sum_{j=i+1}^{n} \frac{\partial f}{\partial x_i}\frac{\partial f}{\partial x_j} u(x_i, x_j) \qquad \textbf{Eq. 7}$$

From Eq. 7 a set of uncertainty propagation equations designed for reflectance calibration uncertainties in atmospherically corrected vegetation indices can be created and are shown in their respective sections below (Miura et al., 1999). Uncertainty estimations for surface reflectance values have been developed during AOP construction and will be rigorously monitored and revised during operations via lab and field calibration and validation activities. Preliminary comparison of simulated and observed uncertainty supports the use of this approach, as seen in **Figure 3** below.

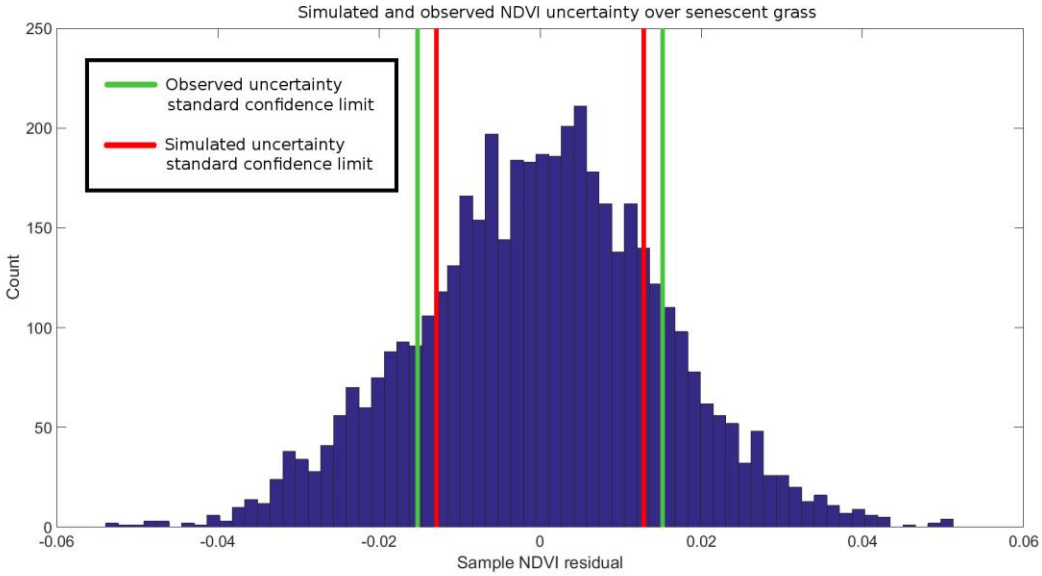

Figure 3. Preliminary comparison of uncertainty predicted by model simulation to uncertainty measured in actual NIS imagery.

In each of the following subsections, uncertainty values are calculated across the range of all possible combinations of input reflectance values and the results presented as surfaces. Some of these surface show certain combinations of reflectance values can result in uncertainty increasing very rapidly. The combinations of values that result in uncertainty rising asymptotically are where two or more of the bands have reflectance values approaching 0.0 or 1.0. While this is theoretically possible, e.g. extremely dark shadows or extremely bright surfaces, it is very unlikely in real world data or practical use cases and would occur only over areas where vegetation indices would be inappropriate or not useful.

6.1.1 NDVI Uncertainty

As NDVI inputs are exclusively L1 NIS directional surface reflectance, NDVI uncertainties are entirely dictated by the reflectance values and uncertainties. Because NDVI is a normalized ratio of two bands, as shown earlier in Eq. 1, NDVI uncertainty varies across the allowed range of NDVI from -1 to 1. The equation for NDVI uncertainty as derived from Eq. 7 is show in Eq. 8 (Huete et al., 1999).

$$u_{cal}^2(NDVI) = \left(\frac{\partial NDVI}{\partial \rho_{NIR}}\right)^2 u_{cal}^2(\rho_{NIR}) + \left(\frac{\partial NDVI}{\partial \rho_{red}}\right)^2 u_{cal}^2(\rho_{red}) + 2\frac{\partial NDVI}{\partial \rho_{NIR}}\frac{\partial NDVI}{\partial \rho_{red}} u_{cal}(\rho_{NIR},\rho_{red}) \quad \textbf{Eq. 8}$$

where

$$\frac{\partial NDVI}{\partial \rho_{NIR}} = \frac{2\rho_{red}}{(\rho_{NIR}+\rho_{red})^2} \quad \textbf{Eq. 9}$$

$$\frac{\partial NDVI}{\partial \rho_{red}} = \frac{-2\rho_{NIR}}{(\rho_{NIR}+\rho_{red})^2} \quad \textbf{Eq. 10}$$

$$\frac{\partial NDVI}{\partial \rho_{NIR}}\frac{\partial NDVI}{\partial \rho_{red}} = \frac{-4\rho_{NIR}\rho_{red}}{(\rho_{NIR}+\rho_{red})^4} \quad \textbf{Eq. 11}$$

From the above equations, it can be seen that error in the NDVI will vary with both the error of the input reflectance and with the actual reflectance values. Error in NDVI has been calculated for all combinations of Red and NIR reflectance values from 5% to 95% for 2%, 5%, and 10% error in those values. The surface plots for the errors are in **Figure 4**, **Figure 5**, and **Figure 6**.

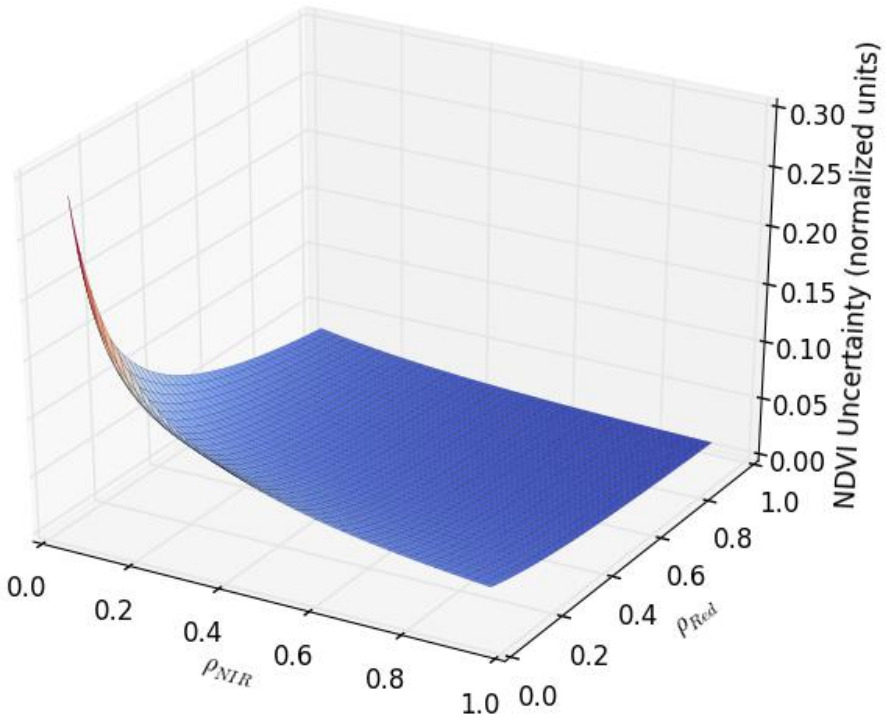

Figure 4. Error in NDVI as a function of input reflectance values with 2% uncertainty.

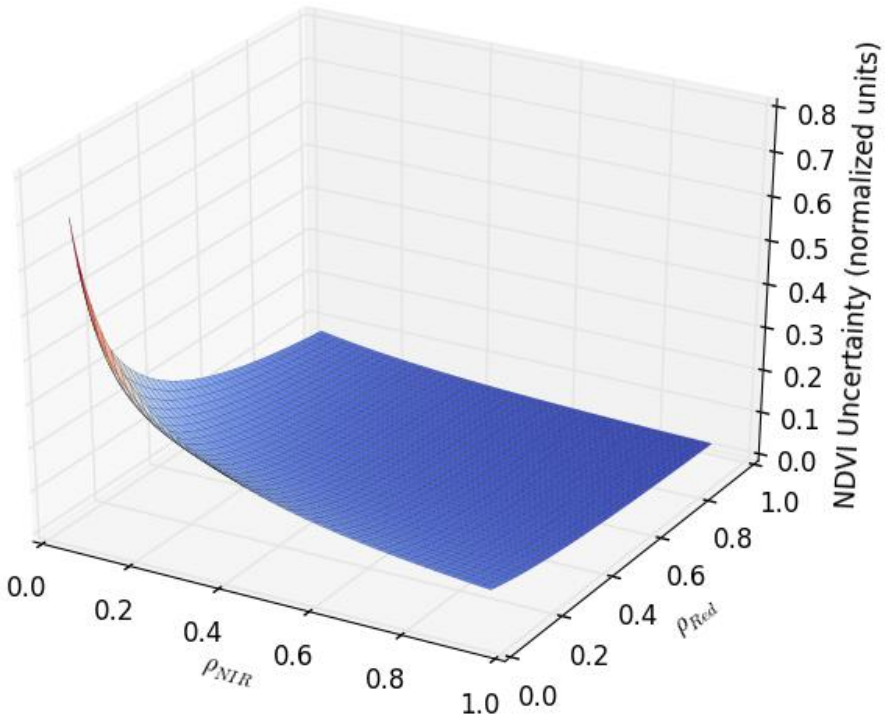

Figure 5. Error in NDVI as a function of input reflectance values with 5% uncertainty.

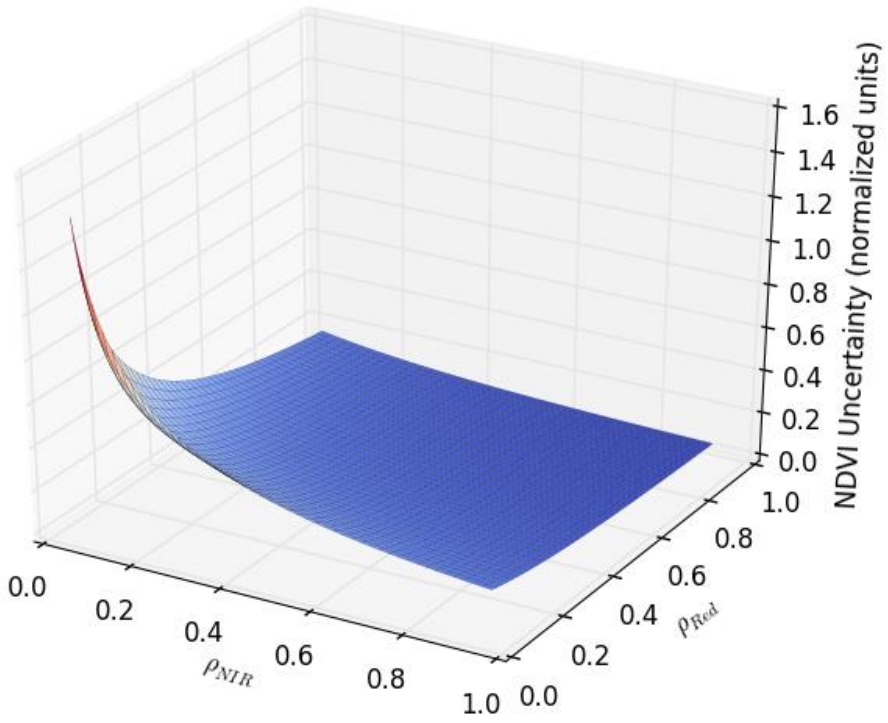

Figure 6. Error in NDVI as a function of input reflectance values with 10% uncertainty.

6.1.2 EVI Uncertainty

As EVI inputs are exclusively L1 NIS directional surface reflectance, EVI uncertainties are entirely dictated by the reflectance values and uncertainties. Because EVI is a normalized ratio of three bands, as shown earlier in Eq. 2, EVI uncertainty varies across the allowed range of EVI from -1 to 1. The equation for EVI uncertainty as derived from Eq. 7 is show in Eq. 12 (Huete et al., 1999).

$$u_{cal}^2(EVI) = \left(\frac{\partial EVI}{\partial \rho_{NIR}}\right)^2 u_{cal}^2(\rho_{NIR}) + \left(\frac{\partial EVI}{\partial \rho_{red}}\right)^2 u_{cal}^2(\rho_{red}) + \left(\frac{\partial EVI}{\partial \rho_{blue}}\right)^2 u_{cal}^2(\rho_{blue}) + 2\frac{\partial EVI}{\partial \rho_{NIR}}\frac{\partial EVI}{\partial \rho_{red}} u_{cal}(\rho_{NIR},\rho_{red}) + 2\frac{\partial EVI}{\partial \rho_{NIR}}\frac{\partial EVI}{\partial \rho_{blue}} u_{cal}(\rho_{NIR},\rho_{blue}) + 2\frac{\partial EVI}{\partial \rho_{red}}\frac{\partial EVI}{\partial \rho_{blue}} u_{cal}(\rho_{red},\rho_{blue}) \quad \textbf{Eq. 12}$$

where

$$\frac{\partial EVI}{\partial \rho_{NIR}} = 2.5\frac{(1+C_1)\rho_{red} - C_2\rho_{blue} + L}{(\rho_{NIR} + C_1\rho_{red} - C_2\rho_{blue} + L)^2} \quad \textbf{Eq. 13}$$

$$\frac{\partial EVI}{\partial \rho_{red}} = 2.5\frac{-\{(1+C_1)\rho_{NIR} - C_2\rho_{blue} + L\}}{(\rho_{NIR} + C_1\rho_{red} - C_2\rho_{blue} + L)^2} \quad \textbf{Eq. 14}$$

$$\frac{\partial EVI}{\partial \rho_{blue}} = 2.5\frac{C_2(\rho_{NIR} - \rho_{red})}{(\rho_{NIR} + C_1\rho_{red} - C_2\rho_{blue} + L)^2} \quad \textbf{Eq. 15}$$

From the above equations, it can be seen that error in the EVI will vary with both the error of the input reflectance and with the actual reflectance values. Error in EVI has been calculated for all combinations of Red and NIR reflectance values from 5% to 95% for 2%, 5%, and 10% error in those values with the Blue reflectance fixed at 5% with uncertainty values equal to those for Red and NIR. As blue reflectance increases, there are many points where input reflectance values can combine such that EVI becomes undefined due to the construction of its denominator. The surface plots for the uncertainty are in **Figure 7**, **Figure 8**, and **Figure 9**.

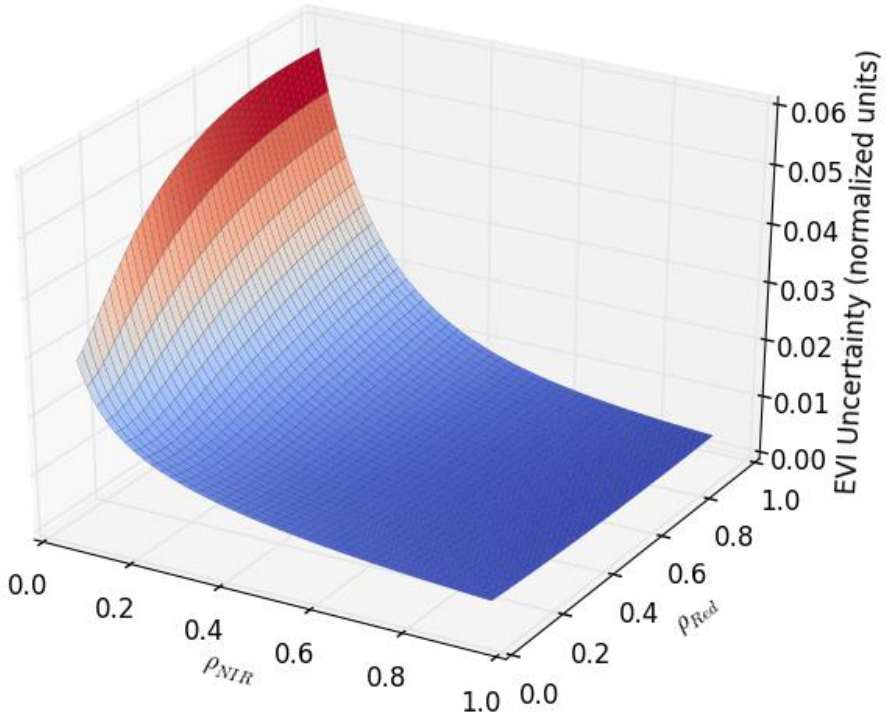

Figure 7. Error in EVI as a function of varying NIR and Red input reflectance values, Blue reflectance of 5%, and all reflectance values with 2% uncertainty.

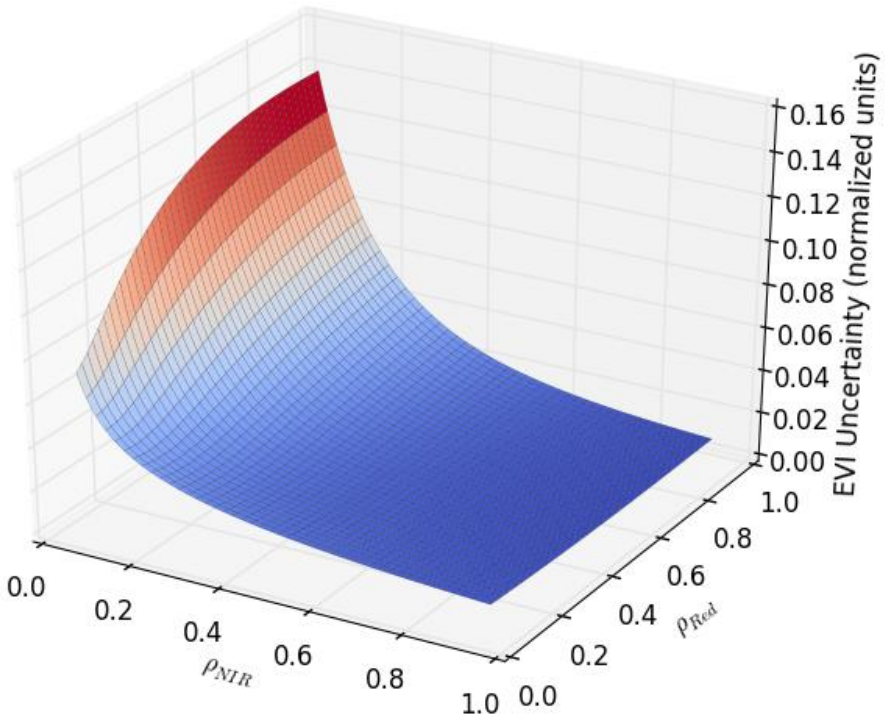

Figure 8. Error in EVI as a function of varying NIR and Red input reflectance values, Blue reflectance of 5%, and all reflectance values with 5% uncertainty.

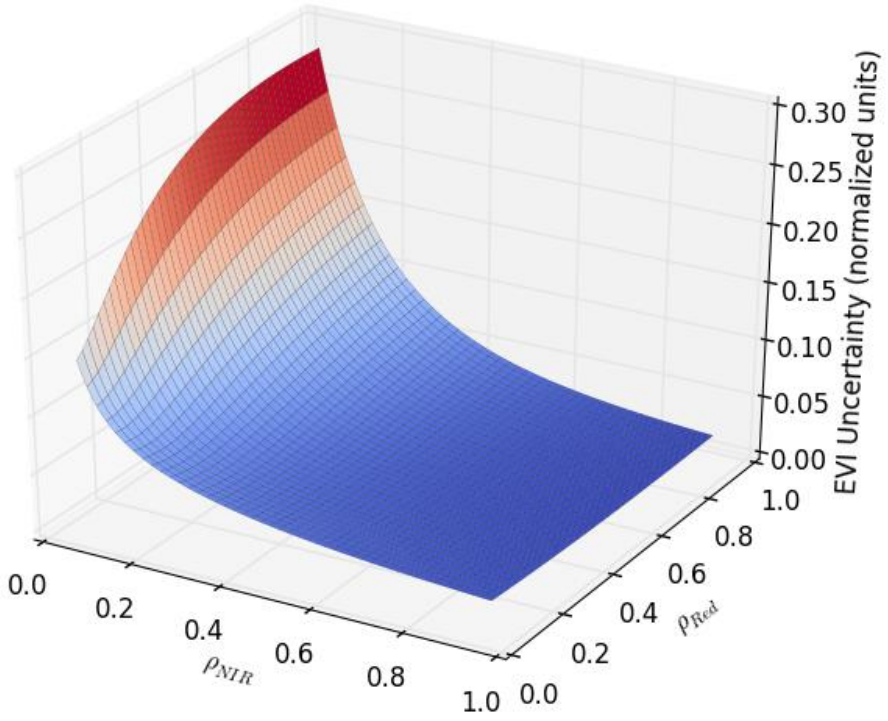

Figure 9. Error in EVI as a function of varying NIR and Red input reflectance values, Blue reflectance of 5%, and all reflectance values with 10% uncertainty.

6.1.3 ARVI Uncertainty

As ARVI inputs are exclusively L1 NIS directional surface reflectance, ARVI uncertainties are entirely dictated by the reflectance values and uncertainties. Because ARVI is a normalized ratio of three bands, as shown earlier in Eq. 3, ARVI uncertainty varies across the allowed range of ARVI from -1 to 1. The equation for ARVI uncertainty as derived from Eq. 7 is show in Eq. 16 (Huete et al., 1999).

$$u_{cal}^2(ARVI) = \left(\frac{\partial ARVI}{\partial \rho_{NIR}}\right)^2 u_{cal}^2(\rho_{NIR}) + \left(\frac{\partial ARVI}{\partial \rho_{red}}\right)^2 u_{cal}^2(\rho_{red}) + \left(\frac{\partial ARVI}{\partial \rho_{blue}}\right)^2 u_{cal}^2(\rho_{blue}) + 2\frac{\partial ARVI}{\partial \rho_{NIR}}\frac{\partial ARVI}{\partial \rho_{red}} u_{cal}(\rho_{NIR},\rho_{red}) + 2\frac{\partial ARVI}{\partial \rho_{NIR}}\frac{\partial ARVI}{\partial \rho_{blue}} u_{cal}(\rho_{NIR},\rho_{blue}) + 2\frac{\partial ARVI}{\partial \rho_{red}}\frac{\partial ARVI}{\partial \rho_{blue}} u_{cal}(\rho_{red},\rho_{blue}) \quad \textbf{Eq. 16}$$

where

$$\frac{\partial ARVI}{\partial \rho_{NIR}} = \frac{2\rho_{rb}}{(\rho_{NIR} + \rho_{rb})^2} \quad \textbf{Eq. 17}$$

$$\frac{\partial ARVI}{\partial \rho_{red}} = \frac{-2(1+\gamma)\rho_{NIR}}{(\rho_{NIR} + \rho_{rb})^2} \quad \textbf{Eq. 18}$$

$$\frac{\partial ARVI}{\partial \rho_{blue}} = \frac{2\gamma\rho_{NIR}}{(\rho_{NIR} + \rho_{rb})^2} \quad \textbf{Eq. 19}$$

From the above equations, it can be seen that error in the ARVI will vary with both the error of the input reflectance and with the actual reflectance values. Error in ARVI has been calculated for all combinations of Red and NIR reflectance values from 5% to 95% for 2%, 5%, and 10% error in those values with the Blue reflectance fixed at 5% with uncertainty values equal to those for Red and NIR. As blue reflectance increases, there are many points where input reflectance values can combine such that ARVI becomes undefined due to the construction of its denominator. The surface plots for the uncertainty are in **Figure 10**, **Figure 11**, and **Figure 12**.

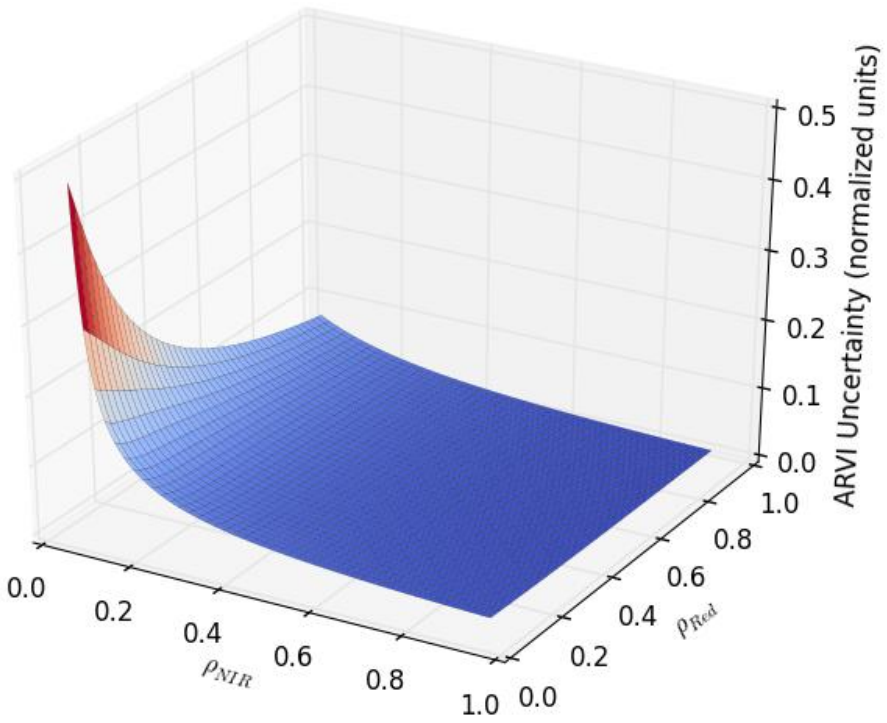

Figure 10. Error in ARVI as a function of varying NIR and Red input reflectance values, Blue reflectance of 5%, and all reflectance values with 2% uncertainty.

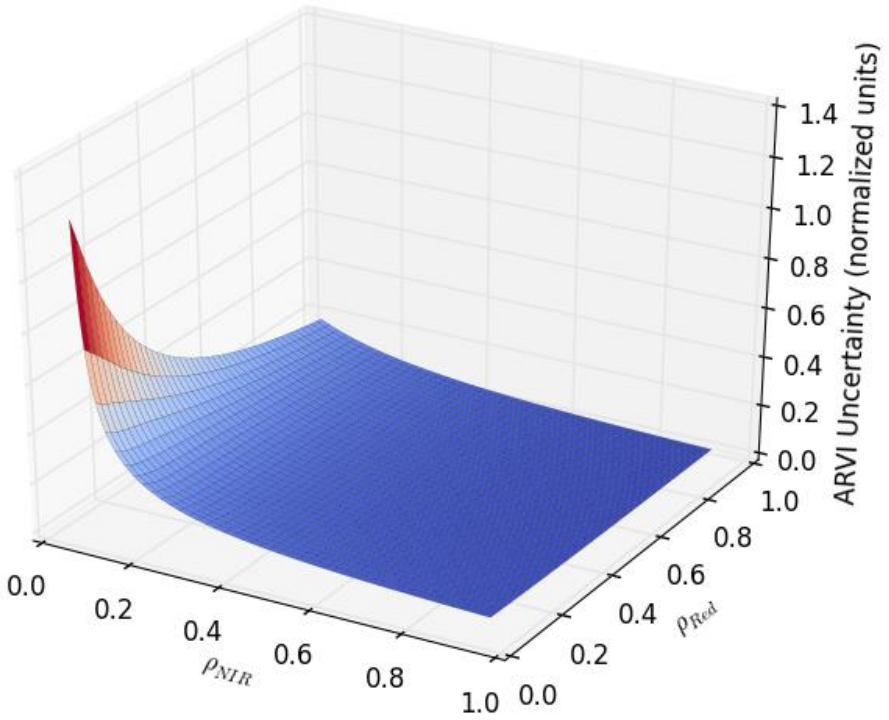

Figure 11. Error in ARVI as a function of varying NIR and Red input reflectance values, Blue reflectance of 5%, and all reflectance values with 5% uncertainty.

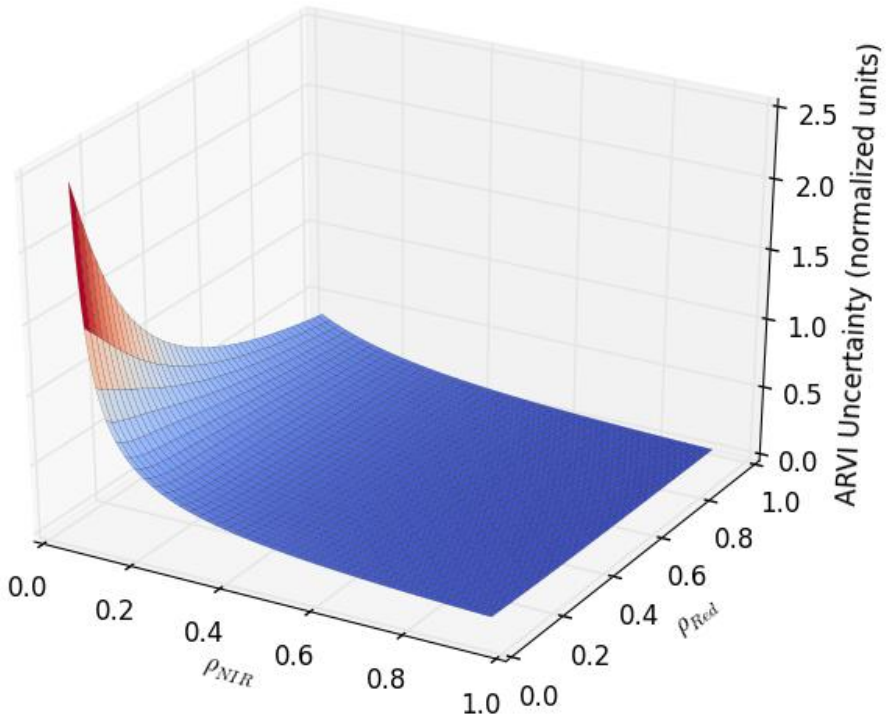

Figure 12. Error in ARVI as a function of varying NIR and Red input reflectance values, Blue reflectance of 5%, and all reflectance values with 10% uncertainty.

6.1.4 Canopy Xanthophyll Uncertainty

As Canopy Xanthophyll (PRI) inputs are exclusively L1 NIS directional surface reflectance, Canopy Xanthophyll uncertainties are entirely dictated by the reflectance values and uncertainties. Because Canopy Xanthophyll is a normalized ratio of three bands, as shown earlier in Eq. 4, Canopy Xanthophyll uncertainty varies across the allowed range of Canopy Xanthophyll from -1 to 1. The equation for PRI uncertainty as derived from Eq. 7 is show in Eq. 20 (Huete et al., 1999).

$$u_{cal}^2(PRI) = \left(\frac{\partial PRI}{\partial \rho_{531}}\right)^2 u_{cal}^2(\rho_{531}) + \left(\frac{\partial PRI}{\partial \rho_{570}}\right)^2 u_{cal}^2(\rho_{570}) + 2\frac{\partial PRI}{\partial \rho_{531}}\frac{\partial PRI}{\partial \rho_{570}} u_{cal}(\rho_{531}, \rho_{570}) \quad \textbf{Eq. 20}$$

where

$$\frac{\partial PRI}{\partial \rho_{531}} = \frac{2\rho_{570}}{(\rho_{531} + \rho_{570})^2} \quad \textbf{Eq. 21}$$

$$\frac{\partial PRI}{\partial \rho_{570}} = \frac{-2\rho_{531}}{(\rho_{531}+\rho_{570})^2} \qquad \textbf{Eq. 22}$$

$$\frac{\partial PRI}{\partial \rho_{531}}\frac{\partial PRI}{\partial \rho_{570}} = \frac{-4\rho_{531}\rho_{570}}{(\rho_{531}+\rho_{570})^4} \qquad \textbf{Eq. 23}$$

From the above equations, it can be seen that error in the PRI will vary with both the error of the input reflectance and with the actual reflectance values. Error in PRI has been calculated for all combinations of ρ_{570} and ρ_{531} reflectance values from 5% to 95% for 2%, 5%, and 10% error in those values. The surface plots for the errors are in **Figure 13**, **Figure 14**, and **Figure 15**.

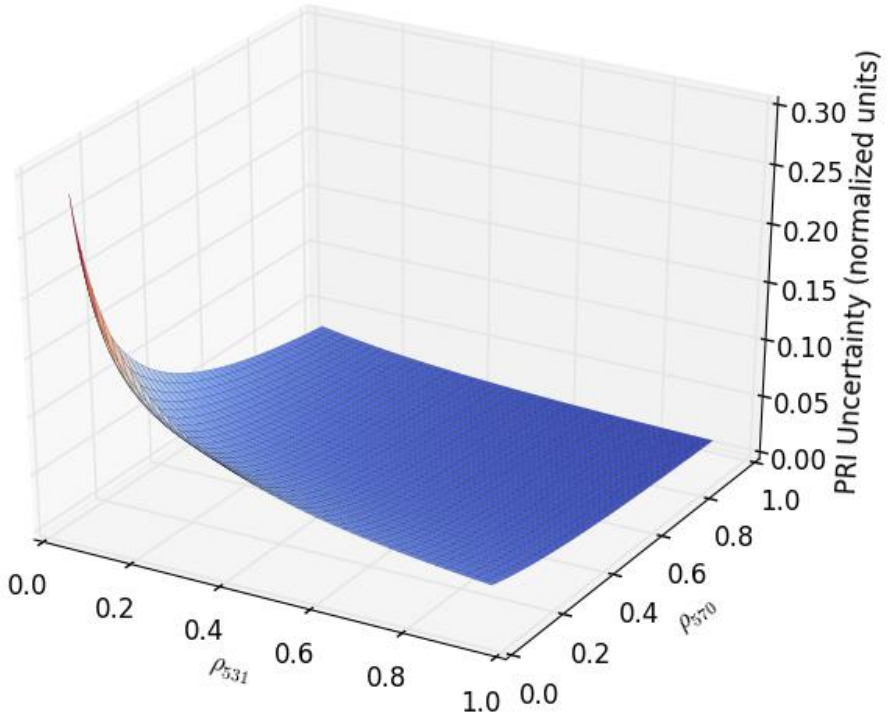

Figure 13. Error in PRI as a function of input reflectance values with 2% uncertainty.

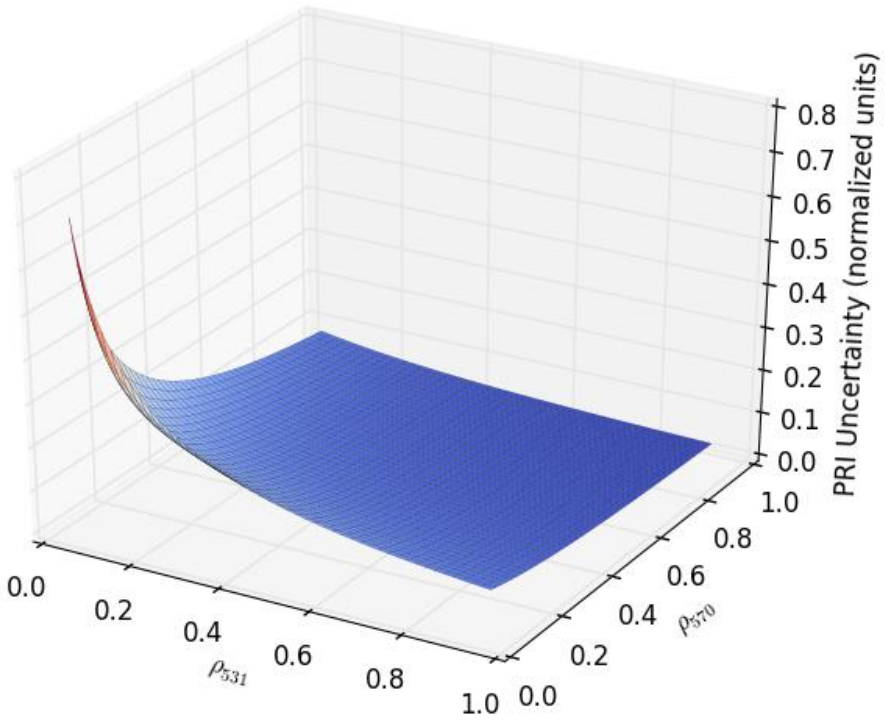

Figure 14. Error in PRI as a function of input reflectance values with 5% uncertainty.

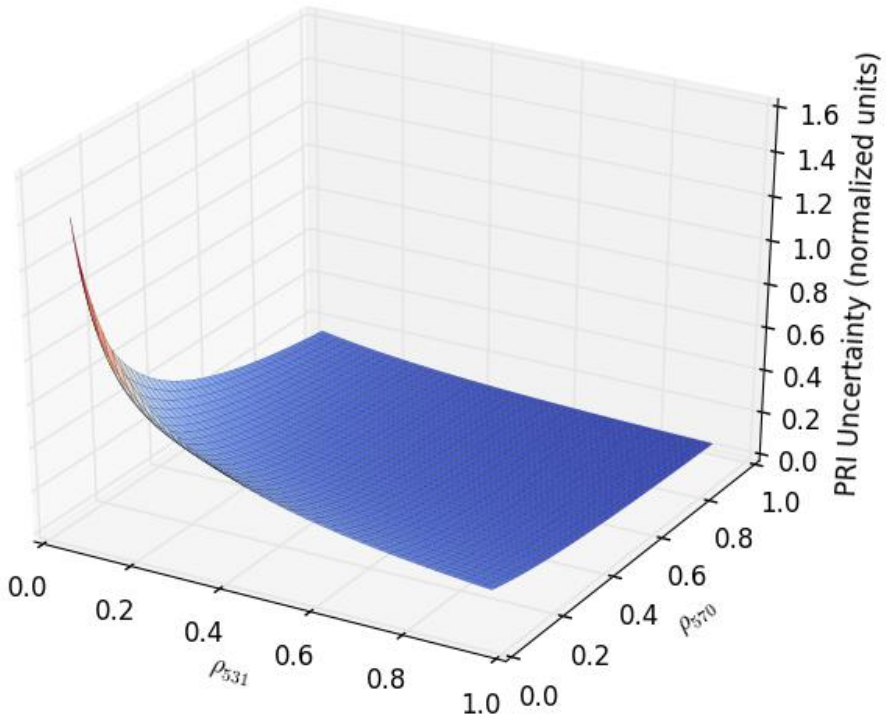

Figure 15. Error in PRI as a function of input reflectance values with 10% uncertainty.

6.1.5 Canopy Lignin Uncertainty

As Canopy Lignin (NDLI) inputs are exclusively L1 NIS directional surface reflectance, Canopy Lignin uncertainties are entirely dictated by the reflectance values and uncertainties. Because Canopy Lignin is a normalized ratio of three bands, as shown earlier in Eq. 5, Canopy Lignin uncertainty varies across the allowed range of Canopy Lignin from -1 to 1. The equation for NDLI uncertainty as derived from Eq. 7 is show in Eq. 24 (Huete et al., 1999).

$$u_{cal}^2(NDLI) = \left(\frac{\partial NDLI}{\partial \rho_{1754}}\right)^2 u_{cal}^2(\rho_{1754}) + \left(\frac{\partial NDLI}{\partial \rho_{1680}}\right)^2 u_{cal}^2(\rho_{1680}) + 2\frac{\partial NDLI}{\partial \rho_{1754}}\frac{\partial NDLI}{\partial \rho_{1680}} u_{cal}(\rho_{1754},\rho_{1680}) \quad \textbf{Eq. 24}$$

where

$$\frac{\partial NDLI}{\partial \rho_{1754}} = \frac{-2\ log\left(\frac{1}{\rho_{1680}}\right)}{\rho_{1754}\ ln(10)\left(log\left(\frac{1}{\rho_{1754}}\right) + log\left(\frac{1}{\rho_{1680}}\right)\right)^2} \quad \textbf{Eq. 25}$$

$$\frac{\partial NDLI}{\partial \rho_{1680}} = \frac{2\ log\left(\frac{1}{\rho_{1754}}\right)}{\rho_{1680}\ ln(10)\left(log\left(\frac{1}{\rho_{1754}}\right) + log\left(\frac{1}{\rho_{1680}}\right)\right)^2} \quad \textbf{Eq. 26}$$

$$\frac{\partial NDLI}{\partial \rho_{1754}}\frac{\partial NDLI}{\partial \rho_{1680}} = \frac{-4log\left(\frac{1}{\rho_{1680}}\right)\left(\frac{1}{\rho_{1754}}\right)}{\rho_{1754}\rho_{1680}\ ln^2(10)\left(log\left(\frac{1}{\rho_{1754}}\right) + log\left(\frac{1}{\rho_{1680}}\right)\right)^4} \quad \textbf{Eq. 27}$$

From the above equations, it can be seen that error in the NDVI will vary with both the error of the input reflectance and with the actual reflectance values. Error in NDVI has been calculated for all combinations of Red and NIR reflectance values from 5% to 95% for 2%, 5%, and 10% error in those values. The surface plots for the errors are in **Figure 16**, **Figure 17**, and **Figure 18**.

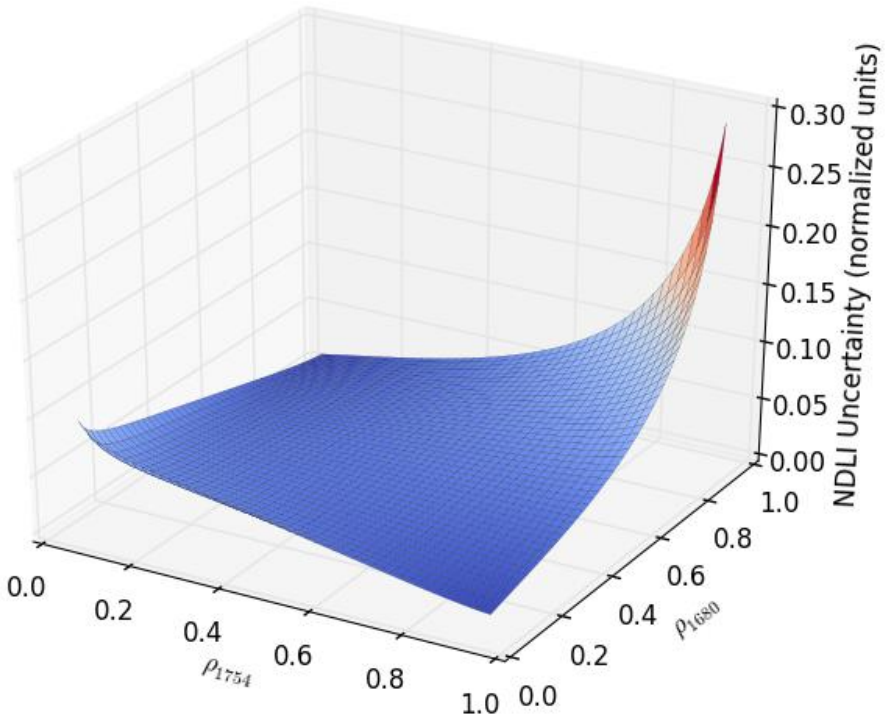

Figure 16. Error in NDLI as a function of input reflectance values with 2% uncertainty.

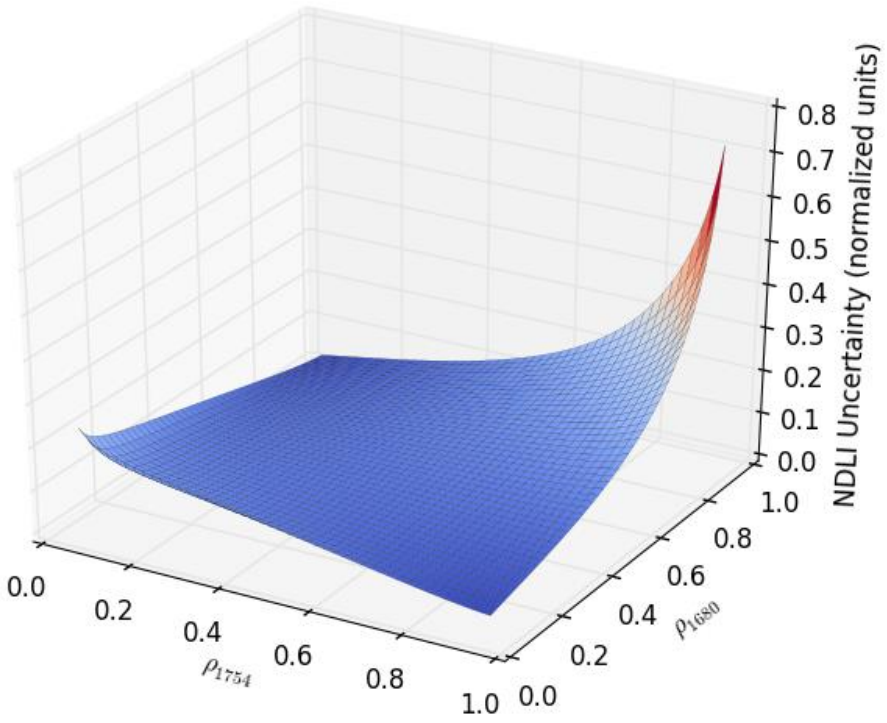

Figure 17. Error in NDLI as a function of input reflectance values with 5% uncertainty.

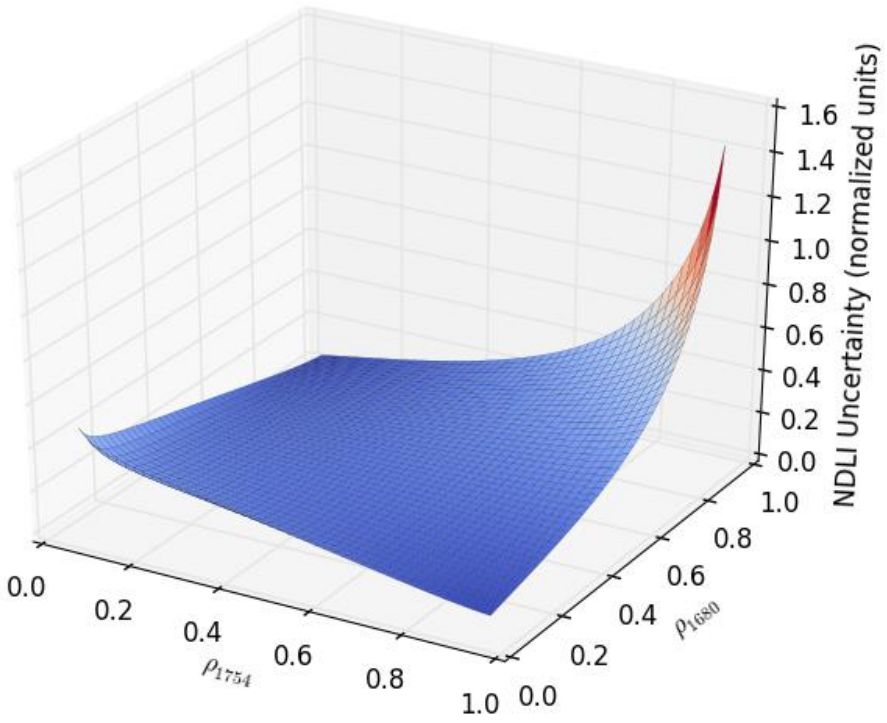

Figure 18. Error in NDLI as a function of input reflectance values with 10% uncertainty.

6.2 Reported Uncertainty

Currently, no uncertainty is reported with the Vegetation Index product(s). In the future, the uncertainty associated with each pixel will be reported in a separate raster of uncertainty values. The uncertainty will be obtained from the reflectance errors propagated through the appropriate index formulae as was done for the surfaces in 6.1. It should be noted that this form of communicating uncertainty in remote sensing products differs from the historic approach of providing a single RMSE value for reporting error in a raster. Although common, the single-value form of reporting uncertainty has faced criticism for not describing the spatial pattern of uncertainty within the product and for not providing information on the context of contributing error. NEON, operating in data acquisition, processing, and distribution roles, has a unique opportunity to create and provide superior and more detailed information on uncertainty within given data products, such as vegetation indices, to researchers and end users.

7 VALIDATION AND VERIFICATION

7.1 Algorithm Validation

As the algorithms are already defined and agreed upon in the remote sensing disciplines, no algorithm validation activities are planned. If newer, more preferable indices arise they may be added to the NEON Data Products Catalog, complementing or replacing other vegetation indices as necessary.

7.2 Data Product Validation

Vegetation index products will be validated against similar data products derived from other well-established and calibrated sensor programs such as Landsat. NIS imagery will be spatially aggregated and spectrally resampled to match the wider bandpasses and larger 30 m pixels of Landsat data. Not all NEON vegetation indices can be validated against all other candidate validation datasets. Most multispectral sensors do not have the required bands for all NEON vegetation index products.

7.3 Data Product Verification

Data product verification for vegetation indices will be accomplished using directly measured field reflectance spectra. NEON AOP operations include periodic acquisition of field spectra during data acquisition flights. The field spectra will be used to verify L1 directional reflectance products as well as vegetation index products.

8 FUTURE MODIFICATIONS AND PLANS

A more sophisticated approach for selecting the NIS bands to be used in index calculations is currently in development. The new approach will use a weighted combination of many NIS bands to optimally cover the range of the spectral feature of interest. This will result in an implementation of the standard vegetation index algorithms in a way making them most comparable between sensors, robust to noise in individual bands, more robust to atmospheric correction error, and better able to properly capture the index value for different types of vegetation when the exact location of the spectral feature of interest differs somewhat from the average.

An additional index, Normalized Difference Nitrogen Index (NDNI) will be added to this ATBD and to the collection of Vegetation Index (VI) products.

The modeled, predicted uncertainty ranges in this document will be continuously validated against measured uncertainty in actual NIS data as it is collected. This document will be updated accordingly with the results and plots of those comparisons.

9 BIBLIOGRAPHY

Fourty, T., et al. "Leaf Optical Properties with Explicit Description of Its Biochemical Composition: Direct and Inverse Problems." *Remote Sensing of Environment* 56 (1996): 104-117.

Gamon, J., J. Penuelas, and C. Field. "A Narrow-Waveband Spectral Index That Tracks Diurnal Changes in Photosynthetic Efficiency." *Remote Sensing of Environment* 41 (1992): 35-44.

Gamon, J., L. Serrano, and J. Surfus. "The Photochemical Reflectance Index: An Optical Indicator of Photosynthetic Radiation Use Efficiency Across Species, Functional Types and Nutrient Levels." *Oecologia* 112 (1997): 492-501.

Huete, A., et al. "Overview of the Radiometric and Biophysical Performance of the MODIS Vegetation Indices." *Remote Sensing of Environment* 83 (2002):195–213.

Kaufman, Y., and D. Tanre. "Atmospherically Resistant Vegetation Index (ARVI) for EOS-MODIS. *IEEE Transactions on Geoscience and Remote Sensing* 30, no. 2 (1992): 261-270.

Melillo, J., J. Aber, and J. Muratore. "Nitrogen and Lignin Control of Hardwood Leaf Litter Decomposition Dynamics." *Ecology* 63 (1982): 621-626.

Miura, T., Tsend-Ayush, J., & Turner, J. P. "Compatibility Analysis of Multi-Sensor Vegetation Indices Using EO-1 Hyperion Data". 34th International Symposium on Remote Sensing of Environment, ISPRS (2011). Available online at http://www.isprs.org/proceedings/2011/isrse-34/211104015Final00571.pdf

Miura, T., Huete, A. R., and Yoshioka, H. (1999), Evaluation of sensor calibration uncertainties on vegetation indices for MODIS (submitted to IEEE Trans. Geosci.Remote Sens.).

NCSL (1997), American National Standard for Expressing Uncertainty – U.S. Guide to the Expression of Uncertainty in Measurement, ANSI/NCSL Z540-2-1997, National Conference of Standards Laboratories (NCSL), Boulder, CO, 101p.

Rouse, J., R. Haas, J. Schell, and D. Deering. *Monitoring Vegetation Systems in the Great Plains with ERTS.* Third ERTS Symposium, NASA (1973): 309-317.

Serrano, L., J. Penuelas, and S. Ustin. "Remote Sensing of Nitrogen and Lignin in Mediterranean Vegetation from AVIRIS Data: Decomposing Biochemical from Structural Signals." *Remote Sensing of Environment* 81 (2002): 355-364.

Taylor, B. N. and Kuyatt, C. E. (1994), Guidelines for Evaluating and Expressing the

Uncertainty of NIST Measurement Results, NIST Technical Note 1297, 1994 Ed., Gaithersburg, MD, 24p.

USGS, (2013), How does Landsat 8 differ from previous Landsat satellites?, Reston, VA. Available online at http://landsat.usgs.gov/ldcm_vs_previous.php

10 APPENDIX A

IDL code for generating NEON AOP Vegetation Indices:

```
; Set up the VI task
    Task=ENVITask('SpectralIndices')
    ; Define inputs
    Task.Input_Raster = oRaster
    Task.INDEX = ['Normalized Difference Vegetation Index', $
                'Enhanced Vegetation Index', $
                'Atmospherically Resistant Vegetation Index', $
                'Photochemical Reflectance Index', $
                'Normalized Difference Lignin Index']
    ; Define outputs
    ;ThisOutName = file_dirname(oRaster.URI, /mark_dir) + (strsplit(file_basename(oRaster.URI), '.',
/extract))[0] + '_engL2VI.dat'
    ThisOutName = OutPath + (strsplit(file_basename(oRaster.URI), '.', /extract))[0] + '_engL2VI.dat'
    Task.OUTPUT_RASTER_URI = ThisOutName
    ; Run the task
    Task.Execute
```

11 CHANGELOG

N/A